World Scientific
www.worldscientific.com

Effects of Size and Dispersity of Microcrystalline Celluloses on Size, Structure and Stability of Nanocrystalline Celluloses Extracted by Acid Hydrolysis

Qi Liu

*National Engineering Laboratory for Crop Efficient Water Use
and Disaster Mitigation and Key Laboratory of Dryland Agriculture
Ministry of Agriculture, Institute of Environment
and Sustainable Development in Agriculture
Chinese Academy of Agricultural Sciences, Beijing 100081, P. R. China*

*Department of Agriculture, Bio-engineering and Chemistry
University of Liege-Gembloux Agro-Bio Tech, 5030 Belgium*
liuqi@caas.cn

Weiping Hao

*National Engineering Laboratory for Crop Efficient Water Use
and Disaster Mitigation and Key Laboratory of Dryland Agriculture
Ministry of Agriculture, Institute of Environment
and Sustainable Development in Agriculture
Chinese Academy of Agricultural Sciences, Beijing 100081, P. R. China*
haoweiping@caas.cn

Yongguang Yang

*Department of Cancer and Cell Biology
University of Cincinnati College of Medicine
Cincinnati, Ohio 45267, USA*
yangy9@ucmail.uc.edu

Aurore Richel

*Unit of Biological and Industrial Chemistry
University of Liege-Gembloux Agro-Bio Tech, 5030 Belgium*
a.richel@ulg.ac.be

Canbin Ouyang

*Department of Pesticide, Key Laboratory of Pesticide Chemistry
and Application, Institute of Plant Protection
Chinese Academy of Agricultural Sciences
Beijing 100193, P. R. China*
oycb@iccas.ac.cn

Huan Liu

School of Music and Recording Arts
Communication University of China
Beijing 100024, P. R. China
Guor219@163.com

Rui Guo[‡] and Xu Xia[§]

National Engineering Laboratory for Crop Efficient Water Use
and Disaster Mitigation, and Key Laboratory of Dryland Agriculture
Ministry of Agriculture
Institute of Environment and Sustainable Development in Agriculture
Chinese Academy of Agricultural Sciences, Beijing 100081, P. R. China
[‡]*guorui@caas.cn*
[§]*xiaxu@caas.cn*

Jing Yang

Construction Engineering Test Center
Central Research Institute of Building and Construction CO., Ltd.
MCC Group, Beijing 100088, P. R. China
yj001010@126.com

Jiqing Song[¶]

National Engineering Laboratory for Crop Efficient Water Use
and Disaster Mitigation, and Key Laboratory of Dryland Agriculture
Ministry of Agriculture
Institute of Environment and Sustainable Development in Agriculture
Chinese Academy of Agricultural Sciences, Beijing 100081, P. R. China
songjiqing@caas.cn

Dorothée Goffin[¶]

Department of Agriculture, Bio-engineering and Chemistry
University of Liege-Gembloux Agro-Bio Tech, 5030 Belgium
dorothee.goffin@ulg.ac.be

Nanocrystalline celluloses (NCCs) were separated from four commercial microcrystalline celluloses (MCCs) by an acid hydrolysis–sonication treatment. Transmission electron microscopy (TEM), atomic force microscopy (AFM), Fourier transform infrared (FTIR) spectrum, X-ray diffraction (XRD) and thermogravimetric analysis (TGA) were conducted to investigate the NCCs. MCCs with different morphologies and particle sizes showed different aggregation degrees. The aggregation of MCCs followed the order MCC1 > MCC3 > MCC2 > MCC4, which is the same order of the heights of the resulting NCCs. The best uniformity and thermal stability were characterized for NCC3, which was produced by MCC3 with smallest original particle size and good dispersity among the four MCCs. This result suggests that both the original particle size and dispersity of MCCs had significant effects on separated NCCs.

Keywords: Microcrystalline cellulose; acid hydrolysis; nanocrystalline celluloses.

[¶]Corresponding authors.

1. Introduction

Cellulose is an important biopolymer and the most ubiquitous and abundant natural biomacromolecule produced by plants and microorganisms worldwide.[1] Cellulose fibers possess highly advantageous properties, such as low cost, biodegradability, renewability, high specific strength and modulus, low density, easy processability and relatively reactive surface for grafting specific groups.[2] This material is widely used because of its biocompatibility, biological degradability, and sustainability. Microcrystalline celluloses (MCCs) represent novel commercial cellulose and exist as a fine, white, odorless, crystalline powder, which has been used for years in different industries, including cosmetics, food, pharmaceuticals and plastics.[3] Numerous researchers have reported on the preparation and characterization of MCC particles isolated from various cellulosic sources.[4–6]

Producing composite materials with nanocrystalline celluloses (NCCs) reinforcement has been recently attracting increasing attention because of the extraordinary properties of the nanometric size effect for reinforcement. Stable NCC suspensions have been known for more than half a century to be prepared by submitting native cellulose to a harsh sulfuric acid hydrolysis and often followed by ultrasound treatments.[7] NCCs prepared from different types of raw cellulose materials are characterized by methods, such as transmission electron microscopy (TEM), atomic force microscopy (AFM) and scanning electron microscopy (SEM).[8,9] Particles are generally elongated and flat, a few hundreds of nanometers long, 10 nm to 20 nm wide, and a few nanometer thick.[10,11] Several studies about preparation and characterization of NCCs from MCCs also exist.[12,13] Compared with cellulose nanowhiskers extracted from industrial bioresidue, those isolated from MCCs by acid hydrolysis show higher surface charge and crystallinity, as well as lower aggregation and degradation temperature.[12] The high crystallinity of these nanoscale celluloses makes these materials a suitable reinforcement for biocomposites. In addition, Bondeson *et al.*[13] reported that obtaining cellulose nanocrystals/whiskers with a length between 200 nm and 400 nm and a width less than 10 nm is possible with a sulfuric acid concentration of 63.5% (w/w). The effects of hydrolysis conditions and surface charge density,[14] ionic strength[15] and pH[16] on the phase separation behavior and structures of the products have been studied over the past two decades.

Although numerous studies about the effect of hydrolysis conditions and properties of the resulting NCCs have been conducted, comparative studies about acid hydrolysis of MCCs with different morphologies, particle sizes and dispersibilities are few. In this study, we submitted four commercial MCCs to sulfuric acid hydrolysis and examined their morphology and particle size. The shape and size distribution of the resulting NCCs were determined by TEM and AFM. Fourier transform infrared (FTIR) spectrum and X-ray diffraction (XRD) experiments were used to describe material structure and crystallinity. Thermogravimetric analysis (TGA) was conducted to determine thermal stability.

2. Materials and Methods

2.1. *Materials*

The four commercial MCCs used in this work were purchased from Ruibio-bio Company (Germany), Sigma-Aldrich Company (USA), Aladdin Industrial Corporation (China) and Xiya Regent Research Center (China). All other reagents and chemicals were of analytical grade. All experiments were performed with ultrapure water.

2.2. *Preparation of the NCCs*

MCCs were hydrolyzed according to the method described by Revol *et al.*[17] All four samples were treated with 64% sulfuric acid at a temperature of 50°C in a Pro Thermo Shaker NTS-3100 (Rikakikai Co., Ltd, Tokyo, Japan) and a speed of 120 r/min for 40 min. MCC content was 5 wt.%. The bottles with suspension were placed in cold water to quench the reactions. The hydrolyzed samples were washed by centrifugation at 15 000 rpm and 8°C for 15 min with a Heraeus centrifuge (Heraeus Co., Ltd, Germany). Centrifugation was repeated five times before the suspension was dialyzed against ultrapure water for several days to neutrality. The molecular weight cut-off of the dialysis bag ranged from 8000 Da to 14 000 Da. The resulting suspension was then sonicated for 10 min with a JY99-IIDN Ultrasonic Processor (Saifu Experimental Instrument Co., Ltd, Ningbo, China) at an output power of 1100 W to obtain the NCCs. The entire treatment process was performed in an ice bath.

A portion of the each resulting suspension was then freeze-dried with an FD-1 freeze dryer at $-50°C$ (Boyikang Experimental Instrument Co., Ltd, Beijing, China) to obtain the NCC powder. The resulting products were then collected.

2.3. *Characterization*

2.3.1. *Morphology of MCCs*

The cellulose fibers were observed by SEM using a Hitachi S-4800 field emission scanning electron microscope (Hitachi High Technologies America, Inc., USA). The original MCC cellulose fibers were directly used. The samples were coated with gold by an ion sputter coater and were observed under SEM operating at 5 kV.

2.3.2. *Laser particle size analysis of MCCs*

The particle size distributions of all the MCC samples were analyzed using a Malvern Mastersizer 2000 laser-diffraction particle size analyzer (Malvern Instruments Ltd., UK) with Malvern Mastersizer 2000 software. The samples were first measured directly in the original state of aggregation to obtain the mean volume diameter of the aggregated particle size. The primary particle size of the MCCs was achieved by sonication for 10 s. Aggregation degree was calculated from the ratio of the aggregated particle size to the primary particle size.

2.3.3. *Morphology and size of NCCs*

The morphology of the fibers was characterized with both TEM and AFM.

2.3.3.1. TEM
Drops of 0.001 wt.% NCC suspensions were deposited on carbon-coated TEM grids. The samples were then negatively stained with 2% uranyl acetate prior to complete drying and observed under a JEM-1200EX transmission electron microscope (JEOL Ltd., Tokyo, Japan) operating at 80 kV. Images were recorded.

2.3.3.2. AFM
To accurately characterize surface topography and microfibril structure, we obtained surface imaging and particle height distribution using a Mutimode 8 atomic force microscope (Bruker Daltonics Inc., USA). Drops of dilute cellulose NCC suspensions were deposited onto freshly cleaved mica and allowed to dry. AFM observations were carried out operating in nitrogen condition and using a ScanA syst mode. ScanA syst is based on the Bruker-exclusive Peak Force Tapping mode. Tapping mode is speculated to be more suitable than contact mode for imaging polymer surfaces because the AFM tip intermittently contacts the surface, leading to minimized destructive lateral forces that can produce surface artifacts.[19] Therefore, all AFM images were recorded in tapping mode.

2.3.4. *FTIR spectroscopy*

FTIR spectroscopy was used to examine any change in the structure of the cellulose fibers after nanocrystallization treatment. A Thermo Scientific Nicolet iN10 (Thermo Electron Corp., USA) was employed to record the FTIR spectrum of each sample. The dried samples were ground and then blended with KBr before pressing the mixture into ultrathin pellets. Spectral outputs were recorded in the transmittance mode as a function of wave number.

2.3.5. *Powder XRD*

Crystallinities of the MCC and NCC fibers were examined using a Bruker D8 Focus (Bruker AXS Inc., Madison, WI, USA) equipped with a high power point focus $CuK\alpha$ target, graphite monochromator for elimination of $Cuk\beta$ lines, and a Hi-Star General Area Diffraction Detection System area detector for 2D images. High-resolution frames for accurate integration of the diffraction images were recorded. Scattered radiation was detected in the range of $2\theta = 10°$ to $30°$ at a scan rate of $4°/min$.

Crystallinity index (CI) was calculated from the heights of the 200 peak (I_{200}, $2\theta = 22.6°$) and the intensity minimum is between the 200 and 110 peaks (I_{am}, $2\theta = 18°$) with the Segal's method,[20] as shown in Eq. (1). I_{200} represents both crystalline and amorphous material, whereas I_{am} represents the amorphous material.

$$CI(\%) = \left(1 - \frac{I_{am}}{I_{200}}\right) \times 100. \qquad (1)$$

2.3.6. *Thermal analysis*

TGA was performed to compare the degradation characteristics of MCCs with those of NCCs. The thermal stability of each sample was determined using a TGA/DSC 1 thermogravimetric analyzer

(Mettler Toledo Corporation, Schwarzenbach, Switzerland) and analyzed by STAR software (Version 9.3). Runs were performed by weighing out the neat (bulk) surfactant (1 mg to 4 mg) in a 70 μL aluminum cup. The cup was crimped, and a hole was pierced automatically by the instrument just prior to the analysis. The analysis was performed with a constant flux of 40 mL/min of nitrogen to ensure that the change in weight is due to thermal degradation. The temperature of the sample was ramped at a constant rate of 10°C/min, and weight loss or heat evolved was measured against increasing temperature.

3. Results and Discussion

3.1. *Morphology of MCCs*

The morphology of fiber or particle materials is usually observed by SEM.[21–23] The MCC particles were investigated with SEM to determine their shape, size and surface morphology. Figure 1 is a comparison of the SEM images of each MCC prior to hydrolysis. The micrographs show the different shapes of the four MCCs. Figure 1(a) shows that MCC1 are ribbon-like in structure and are composed of long cellulose microfibrils. The microfibrils, which measured about 15 μm to 25 μm wide and 30 μm to 200 μm long, maintain the basic shape of cotton fiber. Figure 1(b) indicates that the particles of MCC2 are nonuniformly sized at about 10 μm to

100 μm. Figure 1(c) shows that MCC3 are more uniform and composed of smaller particles with diameters between 10 μm and 50 μm. Figure 1(d) indicates that the cellulose particles of MCC4 are larger than those of MCC3 and smaller than those of MCC2. The MCCs show diverse shape and size, but these micro-sized cellulose fibers were reported to be composed of strong hydrogen bonding nanofibers,[24] which enable isolation of nanoscale cellulose fibers from the MCCs.

3.2. *Laser particle size analysis*

The size distribution of MCCs was investigated by comparing the mean volume diameter before and after sonication. The test results for each sample and the calculated aggregation degree are given in Table 1. Sonication of the original MCCs for 10 s resulted in a significant reduction in particle size distribution of the MCC sample, especially for MCC1. The different MCCs had different aggregation degrees, which followed the order MCC1 > MCC3 > MCC2 > MCC4 as listed in Table 1. The strong aggregation showed by MCC1 may cause incomplete reaction during hydrolysis when preparing NCCs. However, MCC4 exhibited similar particle size before and after the sonication treatment. This result may be beneficial for sulfuric acid to access the cellulose molecule because MCCs were used to prepare NCCs without any treatment.
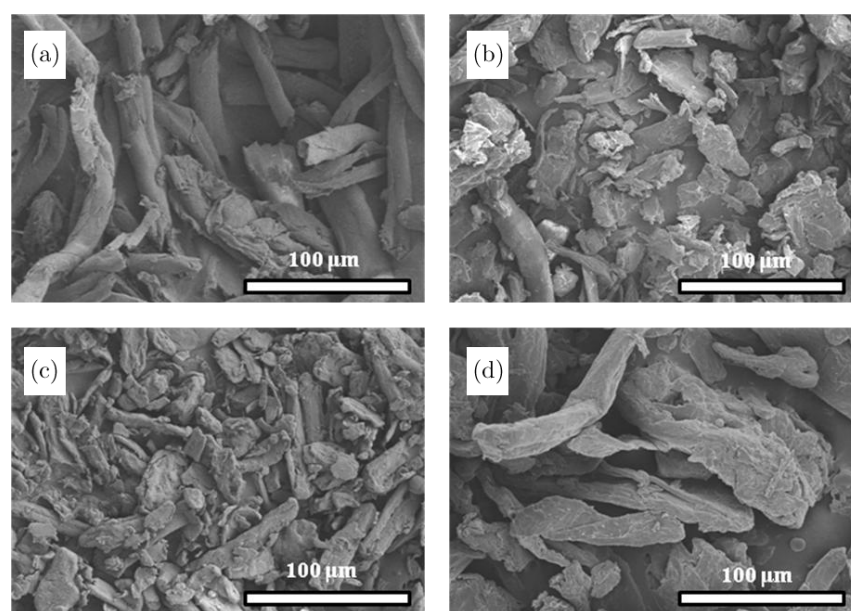

Fig. 1. SEM micrographs of the MCCs: (a) MCC1, (b) MCC2, (c) MCC3 and (d) MCC4.

Table 1. Particle size and aggregation degree of MCCs.

	Mean volume diameter (μm)		
	Before sonication	After sonication	Aggregation degree
MCC1	190.1 $\pm$ 0.22	40.0 $\pm$ 0.14	4.75
MCC2	49.4 $\pm$ 0.06	33.5 $\pm$ 0.67	1.47
MCC3	56.4 $\pm$ 0.09	29.9 $\pm$ 0.06	1.89
MCC4	54.6 $\pm$ 0.04	50.2 $\pm$ 0.12	1.09

Figure 2 presents the particle size distributions of the four MCCs. The size distribution of the samples after sonication showed that the mean volume diameters were 40.0 μm, 33.5 μm, 29.9 μm and 50.2 μm, which is in accordance with the results shown in SEM micrographs. As shown in Figs. 2(b) and 2(c), MCC2 and MCC3 showed a main simple peak with a slight tail. However, the original particle distributions of MCC1 and MCC4 shown in Figs. 2(a) and 2(d) present two or even more peaks. For MCC1, this result was mainly caused by the high aggregation degree of the original particles. MCC4

showed two main peaks at around 35 μm and 100 μm, which may be due to the raw material species or the preparation technology.

3.3. *Morphology and size of NCCs*

3.3.1. *TEM*

Figure 3 shows TEM micrographs of all nanoparticles prepared by sulfuric acid hydrolysis of the four commercial MCCs. The nanoscale particles isolated from MCCs all present an elongated rod shape. The NCCs were approximately 100 nm to 250 nm long and 10 nm to 30 nm wide. NCC4 showed the thinnest width at around 10 nm, whereas all the other three ranged from 20 nm to 25 nm. An evident whisker fraction was observed in Fig. 3(b), which is possibly caused by localized damage created during the process of sonication treatment. Elazzouzi-Hafraoui *et al.*[18] also found this phenomenon in their study of acid hydrolysis of tunicin whiskers. Each image of the samples clearly revealed by negative staining that most particles were composed of several parallel elongated rods. Given the significant
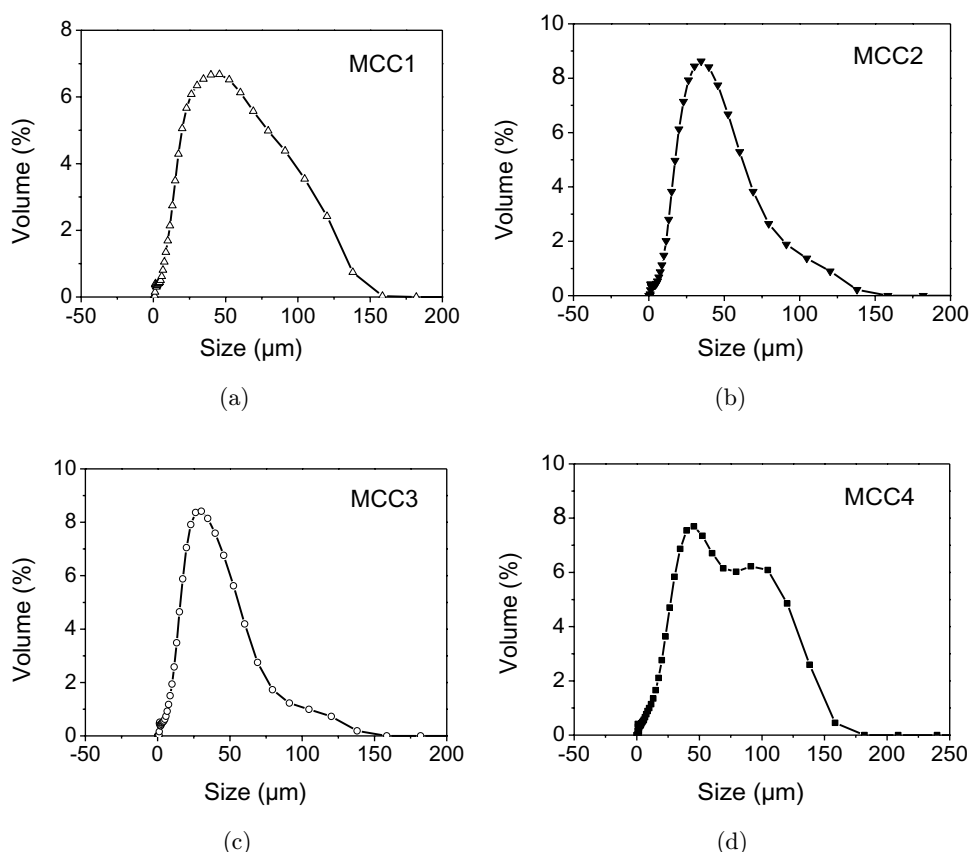

Fig. 2. Particle size distribution of the MCCs: (a) MCC1, (b) MCC2, (c) MCC3 and (d) MCC4.
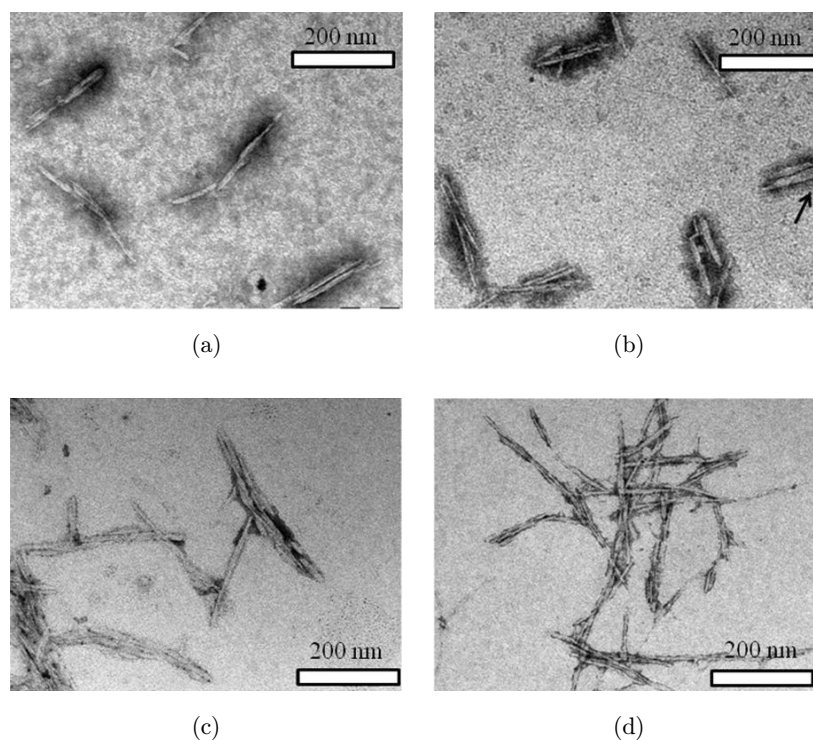
Fig. 3.   TEM micrographs of the NCCs separated from the MCCs: (a) NCC1, (b) NCC2, (c) NCC3 and (d) NCC4.

electrostatic repulsion because of the negative charge of sulfate groups present on the nanocrystal surface after sulfuric acid hydrolysis,[18] this association was attributed to an artificial aggregation during staining and/or drying of the specimens. Among the four micrographs of the NCCs, NCC4 agglomerated to form larger particles in the micron range compared with NCC1, NCC2 and NCC3. This result presents evidence that thinner particles are easier to assemble together.

3.3.2.   *AFM*

Several recent reports have discussed the morphology and crystal structure of NCCs using AFM. Elazzouzi-Hafraoui *et al.*[18] used AFM to study the cellulose surface and determine the nanoparticle thickness by topography measurements of cellulose particles isolated from cotton and tunicin. Images generated in this study using AFM illustrated the morphology and height distribution of NCCs isolated from the four MCCs. The four left-hand images are height images that represent surface topography, and the right-hand images show the particle height from the section analysis in the height image. The height images of Fig. 4 show

AFM images from NCC1 to NCC4 particles deposited onto freshly cleaved mica surfaces. Despite sonication of the suspensions performed before spreading on mica, some aggregation was observed on certain parts of the surface. Statistical analysis of the section in terms of height distribution could lead to inconclusive results, which are most probably due to particle superimposition during drying.[18] The height images showed that the particle height distribution from the section analysis was calculated with a number of better-isolated particles. The height peaks of NCC1 to NCC4 were about 25.8 nm, 19.6 nm, 23.7 nm and 11.5 nm, respectively. NCC3 showed the highest peak among the four images, indicating that this sample had the most uniform particle size distribution. The height images of NCCs showed that height could typically range from 10 nm to 30 nm, which is consistent with the results shown in TEM images. The order of particle height of NCCs resulted in the following trend: NCC1 > NCC3 > NCC2 > NCC4, which is consistent with the order of aggregation degree of MCCs instead of the original particle size. This result indicates that MCCs with lower aggregation degrees tend to produce narrower NCC particles during acid hydrolysis.

3.4. *FTIR spectra*

The structure change of the polymer materials are generally determined by FTIR technology.[25,26] The four MCCs and the corresponding NCCs were analyzed using FTIR to determine the various chemical changes present during hydrolysis. The FTIR spectrum of each sample is shown in Fig. 5. The FTIR spectra of the four MCCs and the corresponding NCCs were highly similar to each other. The band at $1640\,cm^{-1}$ was assigned to the absorbed water. The
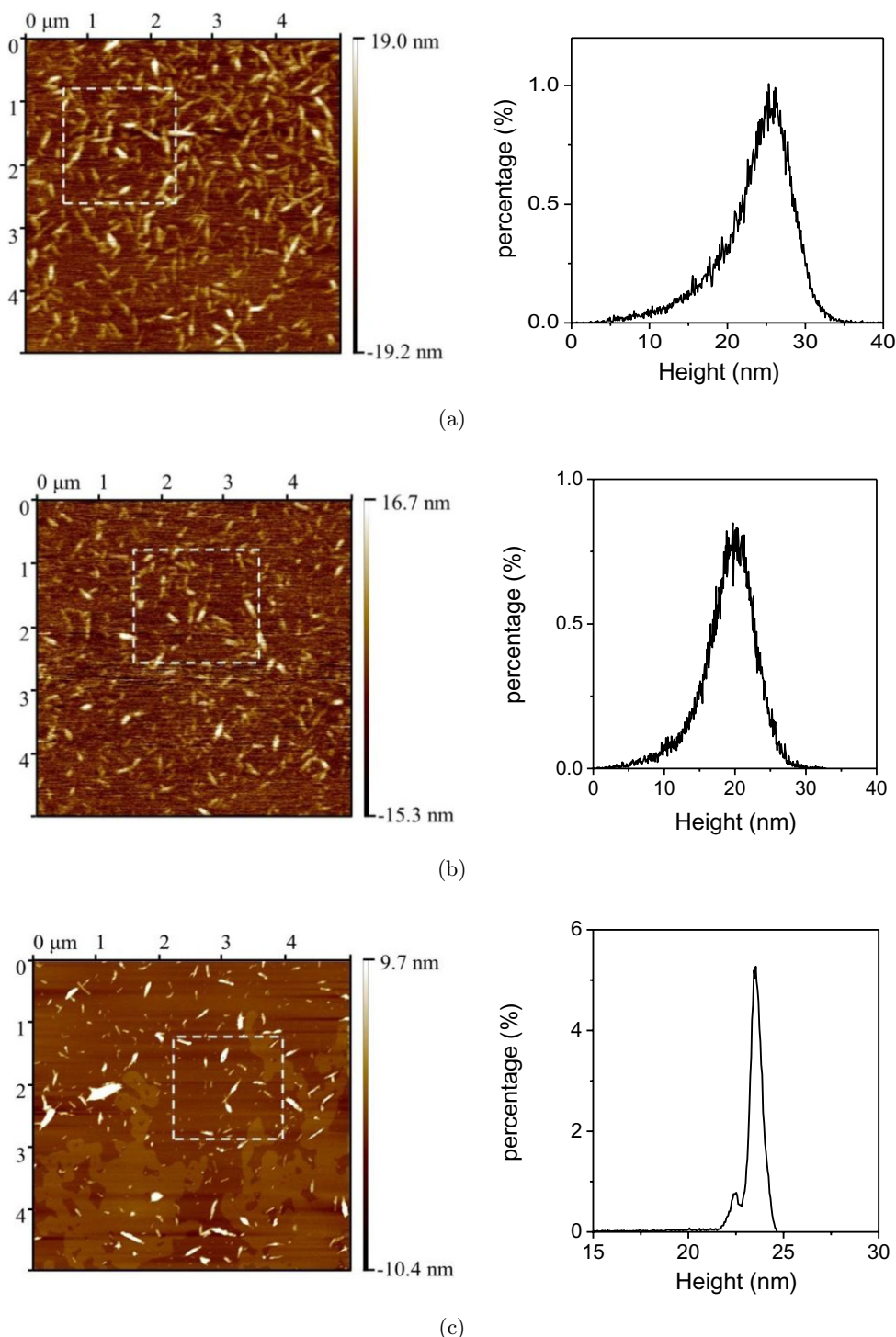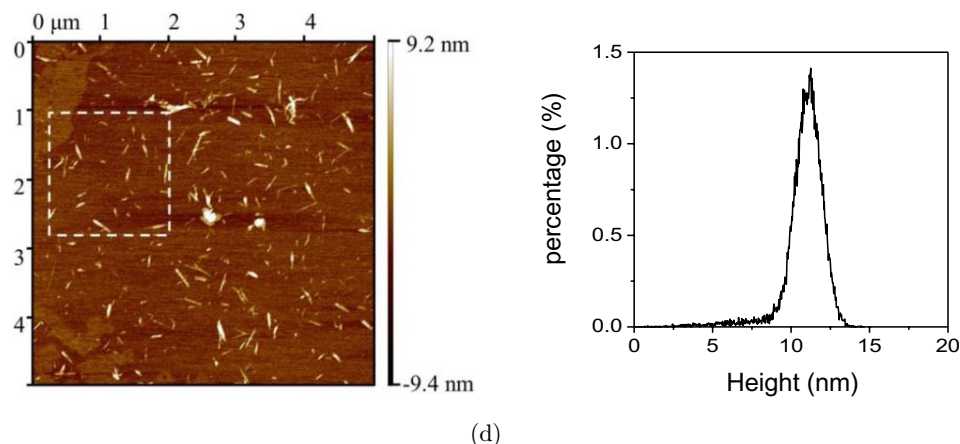

(a)

(b)

(c)

Fig. 4.   AFM images and particle height distribution of NCCs: (a) NCC1, (b) NCC2, (c) NCC3 and (d) NCC4.

(d)

Fig. 4. (*Continued*)

spectra of the samples were dominated by the peaks at $3430\,cm^{-1}$ to $3478\,cm^{-1}$ and $1059\,cm^{-1}$, reflecting the stretching vibrations of O–H and C–O, respectively. The bands at $1061\,cm^{-1}$ and $897\,cm^{-1}$ are associated with C–O stretching and C–H deformation of glucose rings.[8] The absorption peaks at 1642,

1429, 1376, 1163 and $1038\,cm^{-1}$ are normalized with regard to the cellulose peak at $897\,cm^{-1}$.[27] The peaks at around $3400\,cm^{-1}$ in the spectra represent hydroxy stretching. The similar intensity of the aforementioned cellulose peaks in both of MCCs and NCCs indicated that the basic structure did not
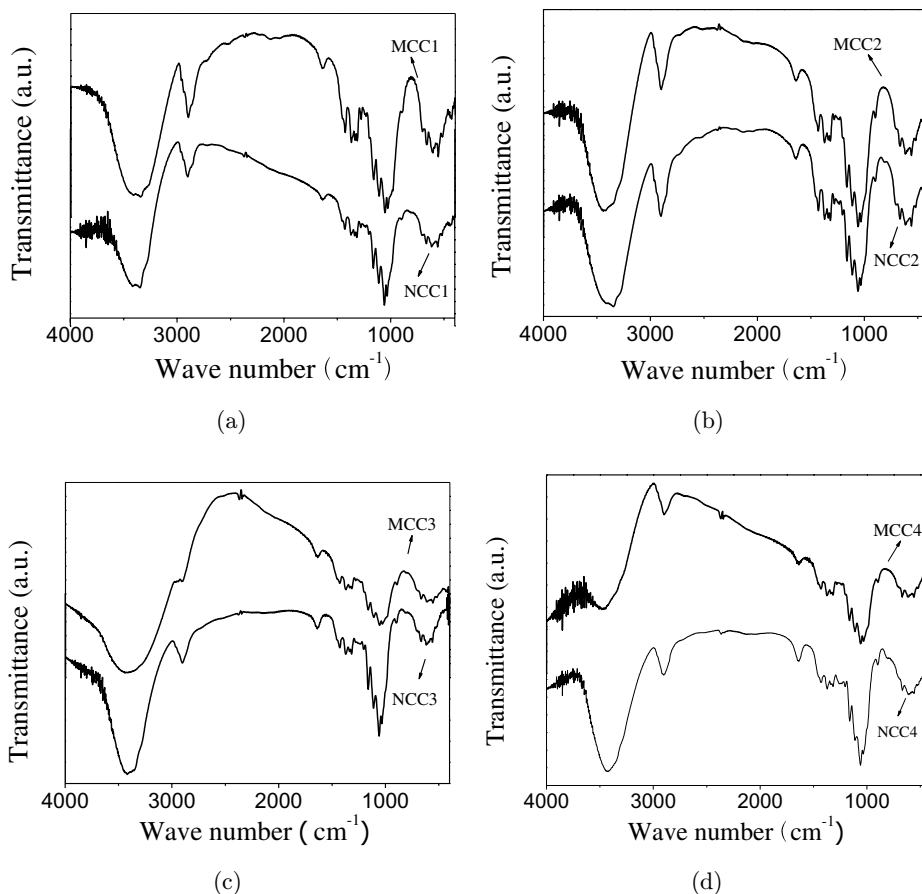

Fig. 5. FTIR spectra of MCCs and NCCs: (a) MCC1 and NCC1, (b) MCC2 and NCC2, (c) MCC3 and NCC3 and (d) MCC4 and NCC4.
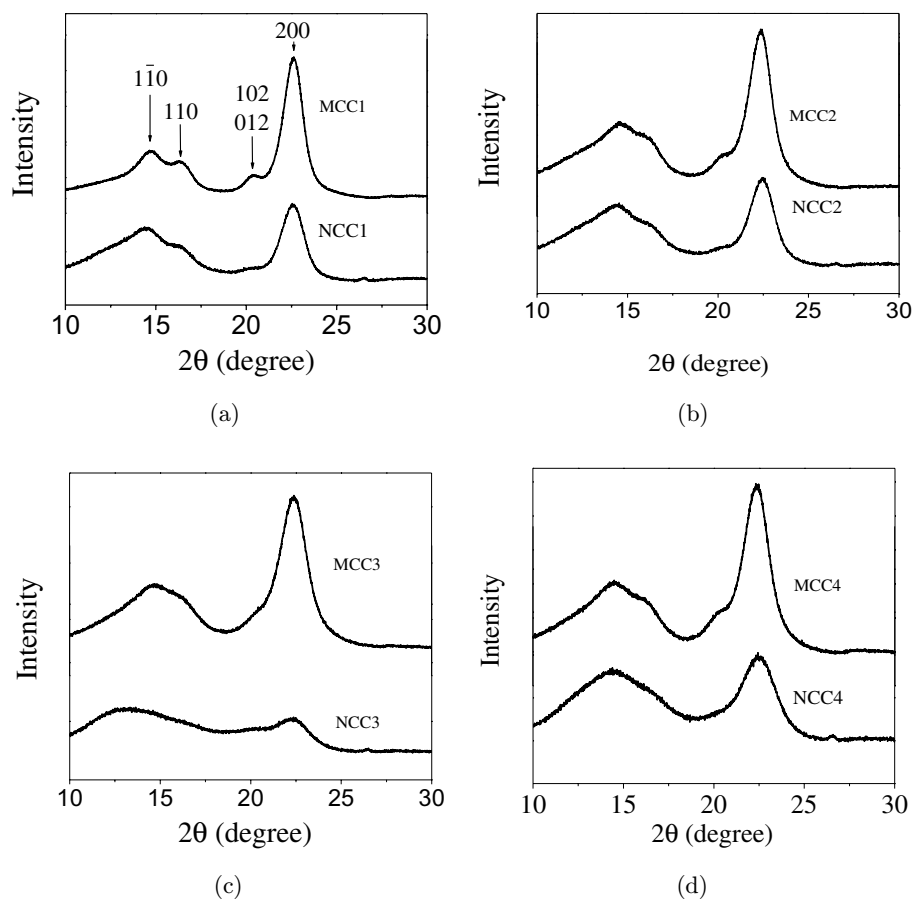
1441014-9

Fig. 6. XRD pattern of MCCs and NCCs: (a) MCC1 and NCC1, (b) MCC2 and NCC2, (c) MCC3 and NCC3 and (d) MCC4 and NCC4.

change during nanocrystallization. However, certain imperceptible changes could be observed by comparing the spectra of each MCC and NCC. Amorphous regions are "dissolved" by acid attack, and the absorption peak at $897\,cm^{-1}$ of glucose rings decreased slightly in the NCC spectra. The shape change of the stretching peak that represents the hydroxy group was also found in the FTIR spectra. The peaks of O–H at $3430\,cm^{-1}$ to $3478\,cm^{-1}$ in the spectra of four MCCs were wider and bigger than those of NCCs. After acid hydrolysis, the bands shifted to a higher frequency area, indicating the decrease of hydrogen bond during this treatment process.

3.5. *X-ray analysis*

XRD studies of the MCC and NCC fibers were performed to investigate the crystalline feature of each cellulose sample. Figure 6 and Table 2 show the XRD patterns and the crystallinities of each MCC and NCC sample. Five diffraction rings or arcs, namely

($1\bar{1}0$), (110), (102/012), (200) and (040), were recognized in all samples. These rings or arcs are characteristics of cellulose I that are based on the monoclinic indexation by Sugiyama *et al.*[28] All patterns of the NCC samples showed peaks around $2\theta = 16.5°$ and $22.5°$, which were speculated to represent the typical cellulose I structure,[29] thus indicating that the crystal properties were not altered during hydrolysis. The crystallinities in the original four MCC fibers were 85.3%, 78.4%, 75.8% and 76.9%. However, an evident decrease in crystallinity was observed in the NCC patterns. This reduction of

Table 2. Crystallinities of the MCCs and NCCs.

	Crystallinities index (%)			
	1	2	3	4
MCCs	85.3	78.4	75.8	76.9
NCCs	69.5	64.9	23.7	48.0
Reduced percentage (%)	18.5	17.2	68.7	37.6

crystallinity was caused by the high concentration of sulfuric acid during nanocrystallization. The breakdown of the cellulose chains, as well as their entanglement and agglomeration, has been proven to be significantly dependent on the acid concentration used.[3] The crystallinities of NCCs are reduced by 18.5%, 17.2%, 68.7% and 37.6%, respectively, compared with those of relevant MCCs. The MCC3 sample was destroyed most seriously, which may be because the smallest original particles of the sample provide the highest superficial area for sulfuric attack.

3.6. *TGA*

Although the thermal properties could be studied through computational and theoretical chemistry,[30,31] TGA is widely used to test the thermal stability. Investigation on the thermal properties of the fibers is important to estimate their applicability for biocomposite processing, in which the processing temperature for thermoplastic polymers rises above

200°C.[8] Figure 7 shows the TGA curves of all MCCs and NCCs. All TGA curves showed an initial small drop between 50°C and 150°C, which corresponded to a mass loss of approximately 5% absorbed moisture. The dominant decomposition peaks of MCCs, which were observed at around 330°C, accounted for the pyrolysis of cellulose. In contrast to the MCC samples, we observed that the four NCCs all exhibited two stages of degradation. These results clearly illustrated that the thermal stability of the fibers decreased after hydrolysis and sonication treatments. Sonication treatment had slight effect on the thermal decomposition of nanofibers[32]; thus, the decrease in thermal stability was caused by the severe condition of sulfuric acid hydrolysis. Hydrolysis of fibers by H_2SO_4 is a heterogeneous reaction.[33] This reaction is influenced by reaction conditions, such as acid concentration, temperature, time and mechanical agitation, as well as the physical state of the cellulose. Among all these factors, acid concentration is one of the key parameters that determine the resulting
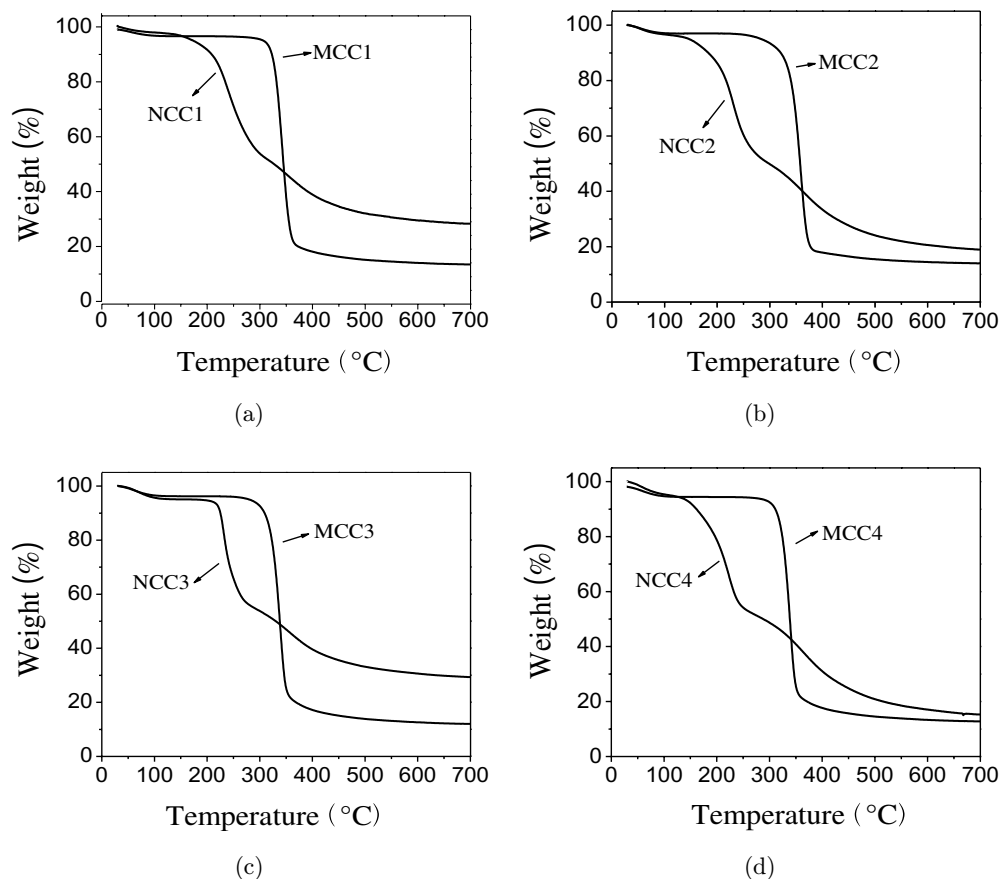

Fig. 7.   TGA curves of MCCs and NCCs: (a) MCC1 and NCC1, (b) MCC2 and NCC2, (c) MCC3 and NCC3 and (d) MCC4 and NCC4.

nature of the fibers.[34] The results are highly consistent with those obtained from FTIR and XRD measurements. Compared with the other three NCCs, NCC3 showed highest degradation temperature, which was approximately 230°C. The high thermal properties of NCC3 may broaden the fields of application of cellulose fibers, especially at temperatures higher than 200°C for biocomposite processing.

4. Conclusion

NCCs were separated from four commercial MCCs by sulfuric acid hydrolysis and then sonicated. The morphology and particle size of MCCs were characterized through SEM and laser particle size analyzer. The results showed different shapes and sizes, and the aggregation degree followed the order MCC1 > MCC3 > MCC2 > MCC4. The resulting NCCs were composed of elongated rods with 100 nm to 250 nm in length and 10 nm to 30 nm in width. The same order of NCC height as the aggregation degree of MCCs indicates that MCCs with lower aggregation degree tend to produce narrower NCC particles during acid hydrolysis process, which were easier to assemble together. Besides the morphology and particle size of NCCs characterized by TEM and AFM, the molecular structure, crystallinity and thermal properties of the nanosized particles were also investigated. The FTIR and XRD results showed that the basic structure and crystal properties of MCCs did not change during the preparation process. However, the harsh hydrolysis condition reduced their crystallinity and decreased the thermal stability to varying degrees. MCC3, which presented the lowest original particle size and good dispersity, produced the most uniform and thermally stable NCC. This result suggests that both particle size and dispersity are key parameters that influence the separation of NCCs.

Acknowledgments

References

1. M. Deng *et al.*, *Mater. Lett.* **63**, 1851 (2009).
2. E. M. Teixeira *et al.*, *Carbohydr. Polym.* **78**, 422 (2009).
3. K. Das *et al.*, *Cellulose* **16**, 783 (2009).
4. T. Virtanen *et al.*, *Cellulose* **19**, 219 (2012).
5. M. S. Jahan *et al.*, *Cellulose* **18**, 451 (2011).
6. R. L. de Oliveira *et al.*, *J. Therm. Anal. Calorim.* **106**, 703 (2011).
7. F. F. Morehead, *Text. Res. J.* **20**, 549 (1950).
8. A. Alemdar and M. Sain, *Bioresour. Technol.* **99**, 1664 (2008).
9. W. Chen *et al.*, *Cellulose* **18**, 433 (2011).
10. R. H. Marchessault, F. F. M. Morehead and M. J. Koch, *J. Colloid. Sci.* **16**, 327 (1961).
11. S. M. Mukherjee and H. J. Woods, *Biochim. Biophys. Acta* **10**, 499 (1953).
12. M. A. Herrera, A. P. Mathew and K. Oksman, *Mater. Lett.* **71**, 28 (2012).
13. D. Bondeson, A. Mathew and K. Oksman, *Cellulose* **13**, 171 (2006).
14. X. M. Dong, J. F. Revol and G. D. Gray, *Cellulose* **5**, 19 (1998).
15. J. Araki and S. Kuga, *Langmuir* **17**, 4493 (2001).
16. E. Belamie, P. Davidson and M. M. Giraud-Guille, *J. Phys. Chem. B* **108**, 14991 (2004).
17. J. F. Revol *et al.*, *Int. J. Biol. Macromol.* **14**, 170 (1992).
18. S. Elazzouzi-Hafraoui *et al.*, *Biomacromolecules* **9**, 57 (2007).
19. D. Bhattacharya, L. T. Germinario and W. T. Winter, *Carbohydr. Polym.* **73**, 371 (2008).
20. L. G. J. M. A. Segal *et al.*, *Text. Res. J.* **29**, 786 (1959).
21. X. Chen, K. Ding and N. Ayres, *Polym. Chem.* **2**, 2635 (2011).
22. X. Chen and N. Ayres, *Macromolecules* **43**, 1341 (2010).
23. X. Chen and N. Ayres, *J. Polym. Sci., A Polym. Chem.* **49**, 3030 (2011).
24. K. Abe and H. Yano, *Cellulose* **17**, 271 (2010).
25. Y. Huang *et al.*, *J. Polym. Sci., A Polym. Chem.* **51**, 5230 (2013).
26. L. Taylor, X. Chen and N. Ayres, *Polym. Int.* **63**, 127 (2014).
27. M. F. Rosa *et al.*, *Carbohydr. Polym.* **81**, 83 (2010).
28. J. Sugiyama, R. Vuong and H. Chanzy, *Macromolecules* **24**, 4168 (1991).
29. Y. Nishiyama, P. Langan and H. Chanzy, *J. Am. Chem. Soc.* **124**, 9074 (2002).

30. G. W. Wang, X. P. Chen and X. Cheng, *Chem.-Eur. J.* **12**, 7246 (2006).

31. P. Wu *et al.*, *Comput. Theor. Chem.* **1030**, 67 (2014).

32. D. Klemm *et al.*, *Comprehensive Cellulose Chemistry, Vol. 1: Fundamentals and Analytical Methods* (Wiley-VCH publication, Weinheim), 1998).

33. Q. Xiang *et al.*, *Appl. Biochem. Biotechnol.* **105**, 505 (2003).

34. M. A. Saïd Azizi Samir *et al.*, *Macromolecules* **37**, 4313 (2004).